Computer Assisted Mechanics and Engineering Sciences, **13**: 427–444, 2006.

Application of a hybrid finite element — Trefftz approach for acoustic analysis

Bert Pluymers, Caroline Vanmaele, Wim Desmet, Dirk Vandepitte
K.U. Leuven, Department of Mechanical Engineering, Division PMA
Celestijnenlaan 300 B, B-3001 Leuven, Belgium

(Received March 17, 2006)

This paper reviews a wave based prediction technique for steady-state acoustic analysis, which is being developed at the K.U. Leuven Noise and Vibration Research group. The method is a deterministic technique based on an indirect Trefftz approach. Due to its enhanced convergence rate and computational efficiency as compared to conventional element based methods, the practical frequency limitation of the technique can be shifted towards the mid-frequency range. For systems of high geometrical complexity, a hybrid coupling between wave based models and conventional finite element (FE) models is proposed in order to combine the computational efficiency of the wave based method with the high flexibility of FE with respect to geometrical complexity of the considered problem domain. The potential to comply with the mid-frequency modelling challenge through the use of the wave based technique or its hybrid variant, is illustrated for some three-dimensional acoustic validation cases.

1. Introduction

At present, the main deterministic numerical modelling techniques for steady-state acoustic analysis are based on element based techniques, such as the finite element method (FEM) [25] and the boundary element method (BEM) [5]. These element based methods describe the dynamic response variables with approximating shape functions, which are not exact solutions of the governing dynamic equations. A major drawback of the methods is their restriction to low-frequency applications because of the excessive size and computational load of the resulting numerical models at higher frequencies [8, 13]. A major advantage is that there are almost no modelling restrictions regarding the geometric complexity of the considered problem. For high-frequency modelling, some alternative, probabilistic techniques such as SEA have been developed [16]. However, there is still a wide mid-frequency range, for which no adequate and mature prediction techniques are available at the moment. In this mid-frequency range, the computational efforts of conventional element based techniques become prohibitively large, while the basic assumptions of the probabilistic techniques are not yet valid.

In recent years, a deterministic wave based method (WBM) has been developed at the KULeuven - Noise and Vibration Research group for steady-state acoustic analysis [4]. The method is based on an indirect Trefftz approach [24], in that the dynamic response variables are expanded in terms of wave functions, which are exact solutions of the governing dynamic equations. In this way, the unknown wave function contribution factors are merely determined by the boundary conditions. This results in small numerical models, which exhibit an enhanced computational efficiency, as compared to the element based methods [20, 21], and, as a result, the WBM is able to tackle problems at higher frequencies (i.e. in the mid-frequency range). A drawback of the WBM is that the geometrical complexity of the considered problem should be moderate, in order to fully benefit from the enhanced computational efficiency.

Hybrid FE-WB methods [9] try to combine the strengths of both the FEM and the WBM. The total problem domain is partitioned into two types of subdomains, namely, large, geometrically

simple subdomains and smaller, geometrically more complex subdomains. The former are modelled with the WBM while for the latter subdomains, the FEM is applied. Expressing continuity conditions along the resulting interfaces between the WB and FE models, yields a hybrid FE-WB model. This hybrid model exhibits the fast convergence characteristics of the WBM and has no restrictions regarding the complexity of the geometrical description of the considered problem [10, 11].

This paper illustrates the potential of both the WBM and the hybrid FE-WB method for some three-dimensional (3D) acoustic validation cases. The WB and the hybrid prediction results are compared with results obtained with the conventional FEM. No comparison is made with respect to the BEM since, due to the densely populated, complex and frequency dependent system matrices, the BEM can hardly compete with the FEM for solving interior acoustic problems. However, the BEM does become an efficient alternative for tackling problems in unbounded domains, especially when taking into account some recent developments which increase the computational efficiency of the method, such as the fast multi-pole BEM [7, 23], the wave boundary elements [17] and the wave number independent BEM [2, 3, 12].

2. The wave based method

This section outlines the basic concepts of the WBM for the analysis of a bounded, steady-state acoustic problem and illustrates the performance of the method by means of a 3D acoustic cavity analysis.

2.1. Acoustic problem definition

Consider a bounded acoustic cavity V, excited by an acoustic volume velocity point source q at position $\mathbf{r_q}$. Pressure, normal velocity and normal impedance boundary conditions are imposed, respectively, at Ω_p, Ω_v and Ω_Z. Assuming that the system is linear, the fluid is inviscid, and the process is adiabatic, the steady-state acoustic pressure $p(\mathbf{r})$ inside the domain is governed by the inhomogeneous Helmholtz equation

$$\nabla^2 p(\mathbf{r}) + k^2 p(\mathbf{r}) = -j\rho_0\omega\,\delta(\mathbf{r},\mathbf{r_q})\,q \tag{1}$$

with $\mathbf{r}$ the position vector $\{x,y,z\}$, $\nabla^2 = \frac{\partial^2}{\partial x^2} + \frac{\partial^2}{\partial y^2} + \frac{\partial^2}{\partial z^2}$ the Laplacian operator, $k = \frac{\omega}{c}$ the acoustic wave number, ω the angular frequency, c the speed of sound, $j = \sqrt{-1}$, ρ_0 the ambient fluid density and δ a Dirac-delta function.

The acoustic boundary conditions are formulated as

- pressure boundary conditions

$$\mathbf{r} \in \Omega_p: \quad R_p\left(p(\mathbf{r})\right) = p(\mathbf{r}) - \bar{p} = 0 \tag{2}$$

  with $\bar{p}$ the applied pressure,

- normal velocity boundary conditions

$$\mathbf{r} \in \Omega_v: \quad R_v\left(p(\mathbf{r})\right) = \mathcal{L}_v(p(\mathbf{r})) - \bar{v}_n = 0 \tag{3}$$

  with $\bar{v}_n$ the applied normal velocity, $\mathcal{L}_v() = \frac{j}{\rho_0\omega}\frac{\partial}{\partial n}()$ the normal velocity operator and $\frac{\partial}{\partial n}$ the derivative in the normal direction,

- and normal impedance boundary conditions

$$\mathbf{r} \in \Omega_Z: \quad R_Z\left(p(\mathbf{r})\right) = \mathcal{L}_v(p(\mathbf{r})) - \frac{p(\mathbf{r})}{\bar{Z}_n} = 0 \tag{4}$$

  with $\bar{Z}_n$ the applied normal impedance.

2.2. Basic WBM concepts

It has been shown by Desmet [4] that the WB methodology converges towards the exact solution, provided that the considered problem domains are convex. In case of non-convex problem domains, partitioning into convex subdomains is required, yielding subdomain interfaces. At these interfaces, continuity conditions are applied [18]. In the formulations described in this paper, the WB domains are considered to be convex.

The steady-state acoustic pressure field $p(\mathbf{r})$ in the bounded, convex acoustic cavity V is approximated as a solution expansion

$$p(\mathbf{r}) \simeq \hat{p}(\mathbf{r}) = \sum_{a=1}^{n_a} p_a \, \Phi_a(\mathbf{r}) + \hat{p}_q(\mathbf{r}) = \mathbf{\Phi}(\mathbf{r}) \, \mathbf{p_a} + \hat{p}_q(\mathbf{r}), \qquad \mathbf{r} \in V. \tag{5}$$

Each function $\Phi_a(\mathbf{r})$ is an acoustic wave function, which exactly satisfies the homogeneous Helmholtz equation

$$\Phi_a(\mathbf{r}\,(x,y,z)) = \begin{cases} \Phi_{a_r}(x,y,z) = \cos(k_{xa_r} x)\, \cos(k_{ya_r} y)\, e^{-jk_{za_r} z}\,, \\ \Phi_{a_s}(x,y,z) = \cos(k_{xa_s} x)\, e^{-jk_{ya_s} y}\, \cos(k_{za_s} z)\,, \\ \Phi_{a_t}(x,y,z) = e^{-jk_{xa_t} x}\, \cos(k_{ya_t} y)\, \cos(k_{za_t} z)\,. \end{cases} \tag{6}$$

Since the only requirement for the wave number components in (6) is that

$$k_{xa_r}^2 + k_{ya_r}^2 + k_{za_r}^2 = k_{xa_s}^2 + k_{ya_s}^2 + k_{za_s}^2 = k_{xa_t}^2 + k_{ya_t}^2 + k_{za_t}^2 = k^2, \tag{7}$$

an infinite number of wave functions (6) can be defined for expansion (5). It is proposed to select the following wave number components,

$$\begin{aligned} (k_{xa_r}\,,\, k_{ya_r}\,,\, k_{za_r}) &= \left(\frac{a_1\pi}{L_x}\,,\, \frac{a_2\pi}{L_y}\,,\, \pm\sqrt{k^2 - \left(\frac{a_1\pi}{L_x}\right)^2 - \left(\frac{a_2\pi}{L_y}\right)^2} \right), \\ (k_{xa_s}\,,\, k_{ya_s}\,,\, k_{za_s}) &= \left(\frac{a_3\pi}{L_x}\,,\, \pm\sqrt{k^2 - \left(\frac{a_3\pi}{L_x}\right)^2 - \left(\frac{a_4\pi}{L_z}\right)^2}\,,\, \frac{a_4\pi}{L_z} \right), \\ (k_{xa_t}\,,\, k_{ya_t}\,,\, k_{za_t}) &= \left(\pm\sqrt{k^2 - \left(\frac{a_5\pi}{L_y}\right)^2 - \left(\frac{a_6\pi}{L_z}\right)^2}\,,\, \frac{a_5\pi}{L_y}\,,\, \frac{a_6\pi}{L_z} \right), \end{aligned} \tag{8}$$

with a_1, a_2, a_3, a_4, a_5 and $a_6 = 0, 1, 2, \ldots$. The dimensions L_x, L_y and L_z represent the dimensions of the (smallest) rectangular box, enclosing the convex problem domain V.

The wave function contributions p_a in (5) are the unknowns and form the vector $\mathbf{p_a}$. The corresponding wave functions (6) are collected in the row vector $\mathbf{\Phi}$.

$\hat{p}_q(\mathbf{r})$ represents a particular solution resulting from the acoustic source term in (1), with source strength q and located at position $(x_q\,,\, y_q\,,\, z_q)$, and is chosen as

$$\hat{p}_q(\mathbf{r}(x,y,z)) = \frac{j\rho\omega q}{4\pi} \frac{e^{-jkr_q}}{r_q} \qquad \text{with} \quad r_q = \sqrt{(x-x_q)^2 + (y-y_q)^2 + (z-z_q)^2}\,. \tag{9}$$

With the use of the proposed pressure expansion (5), the Helmholtz equation (1) is always exactly satisfied, irrespective of the values of the unknown wave function contributions p_a. These unknown wave function contributions are merely determined by the acoustic boundary conditions. Since the boundary conditions are defined at an infinite number of boundary positions, while only

finite sized prediction models are amenable to numerical implementation, the boundary conditions are transformed into a weighted residual formulation

$$\int_{\Omega_v} \tilde{p}\, R_v(\hat{p})\, \mathrm{d}\Omega + \int_{\Omega_Z} \tilde{p}\, R_Z(\hat{p})\, \mathrm{d}\Omega - \int_{\Omega_p} \mathcal{L}_v(\tilde{p})\, R_p(\hat{p})\, \mathrm{d}\Omega = 0. \tag{10}$$

Like in the Galerkin weighting procedure, the weighting function $\tilde{p}$ is expanded in terms of the same set of acoustic wave functions used in the field variable expansion (5). Substitution of the field variable expansion (5) and the weighting function expansion into the weighted residual formulation (10), yields a square matrix equation in the n_a unknown wave function contributions

$$\mathbf{A}\,\mathbf{p_a} = \mathbf{b}. \tag{11}$$

2.3. Model properties

Degrees of freedom: In the WBM methodology, the degrees of freedom (dofs) are the unknown wave function contribution factors $\mathbf{p_a}$.

Problem discretization & approximation functions: Unlike the FEM (see Section 3.1), the construction of a WB model does not require a problem domain discretization into small elements. The only requirement is a partitioning into convex subdomains. However, these convex subdomains can be large and their sizes are independent of frequency, since the wave functions (6), which are used to describe the dynamic response variables inside the subdomains, are exact solutions of the governing dynamic equations. With increasing frequency, the number of wave functions is increased.

Accuracy of secondary variables: For the WBM, there is no additional loss of accuracy for the higher-order derived quantities (e.g. the acoustic velocity) compared to the primary response variables (e.g. the acoustic pressure), because the derivatives of the wave functions are wave functions with identical wavelengths as the primary wave functions.

System matrix properties: The WB system matrices are non-symmetric and fully populated with complex frequency dependent coefficients.

Computational performance & applicability: The small model size of the WBM, together with the high convergence rate, make it a computationally efficient method, which creates opportunities to tackle problems also in the mid- and even high-frequency range [19]. A sufficient condition regarding the problem domain geometry for the WBM to converge, is convexity of the considered subdomains. This restricts application of the WBM to problems with a moderate geometrical complexity. More complex geometries could be modelled, provided that many subdomains are introduced. This would have a disadvantageous effect on the computational efficiency of the method.

2.4. Numerical results

Figure 1 shows a car-like cavity. The air-filled cavity ($c = 340\ \frac{\mathrm{m}}{\mathrm{s}}$, $\rho_0 = 1.225\ \frac{\mathrm{kg}}{\mathrm{m}^3}$) is surrounded with concrete walls Ω_0, which are acoustically rigid. Inside the cavity, two loudspeakers are positioned. The front loudspeaker is used to excite the system and is considered in the numerical models as a normal velocity boundary excitation of $1\ \frac{\mathrm{m}}{\mathrm{s}}$, applied on a small surface Ω_v, corresponding to the loudspeaker membrane. The second loudspeaker is not activated and considered to be rigid in the numerical models.

To compare the performances of the WBM and the FEM, several models of the considered problem are solved. The FE models are solved with LMS/SYSNOISE Rev. 5.6. The WBM routines

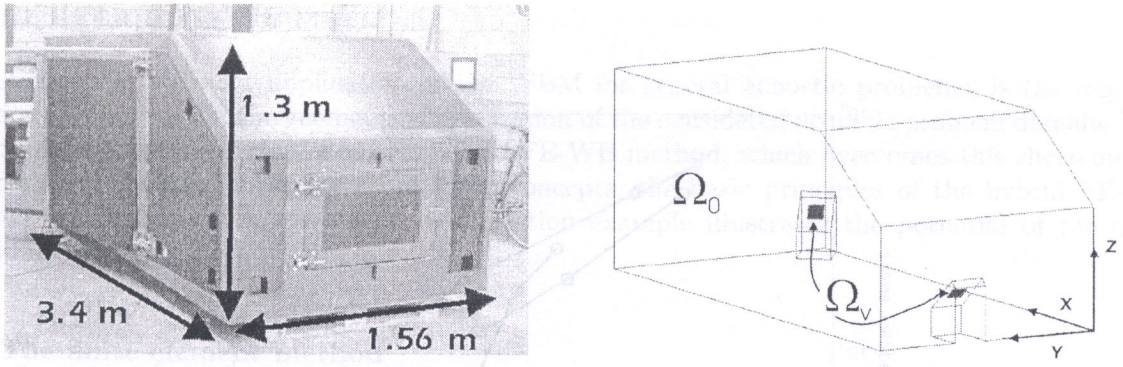

Fig. 1. Concrete car-like cavity, excited by two loudspeakers

are implemented in a C++ code. All calculations are performed on a HP-C3000 UNIX workstation (400 MHz single processor, 2.5 Gb RAM memory, SPECint95 = 31.8, SPECfp95 = 52.4).

Table 1 shows the FE model information for a pressure response calculation at 198 Hz. f_6 and f_{10} indicate the upper limits of the frequency ranges for which the FE mesh includes at least 6 and 10 linear elements per wavelength respectively. t_{Skyline} denotes the CPU time needed for solution of the FE matrix equation using a direct Skyline solver, while t_{QMR} denotes the CPU time for solution with a QMR iterative solver. ϵ is the relative prediction error of the pressure amplitude in a response point inside the cavity $(x, y, z) = (1\,\text{m}, 0.3\,\text{m}, 0.8\,\text{m})$.

$$\epsilon = \left| \frac{p_{\text{prediction}}(\text{Pa}) - p_{\text{reference}}(\text{Pa})}{p_{\text{reference}}(\text{Pa})} \right| . \tag{12}$$

The most detailed FE model (model 5) is used as reference. Table 2 shows the corresponding data for the WB models. The computational load t for the WB models includes both assembly time and solution time of the system of equations, since the WB system matrices are frequency dependent, while the computational loads t_{Skyline} and t_{QMR} include only the time for solving the FE matrix system.

Table 1. FE model information at 198 Hz

	♯ nodes	f_6 (Hz)	f_{10} (Hz)	t_{Skyline} (s)	t_{QMR} (s)	ϵ (%)
1	1886	145	87	0.8		61
2	3301	193	115	2.1	1.0	46
3	10341	238	143	29	6	20
4	25890	367	221	82	23	12
5	72780	521	313	1900	210	

Table 2. WB model information at 198 Hz

	♯ wave functions	♯ convex subdomains	t (s)	ϵ (%)
1	666	17	7	27
2	852	17	13	18
3	1116	17	26	7
4	1674	17	80	2

The pressure convergence plots in Fig. 2 illustrate the enhanced computational efficiency of the WBM in that it exhibits a higher convergence rate than the FEM.

Figure 3 compares the prediction results for the pressure frequency response function (FRF) in the considered point, calculated with the FEM (Skyline solver)(top figure) and the WBM (bottom figure), with the reference solution (dashed line). Both models involve a similar computational load (i.e. 25 CPU seconds per frequency line). The figures indicate that the WBM, unlike the FEM, does not suffer from substantial numerical dispersion [14], in that there is no (significant) shift between the resonance frequencies of the reference solution and the WBM solution, even at higher frequencies [22].

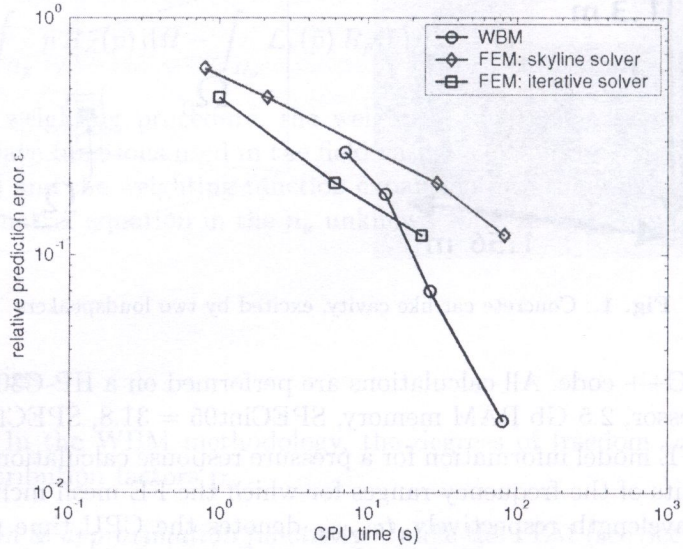

Fig. 2. Pressure convergence plots at 198 Hz

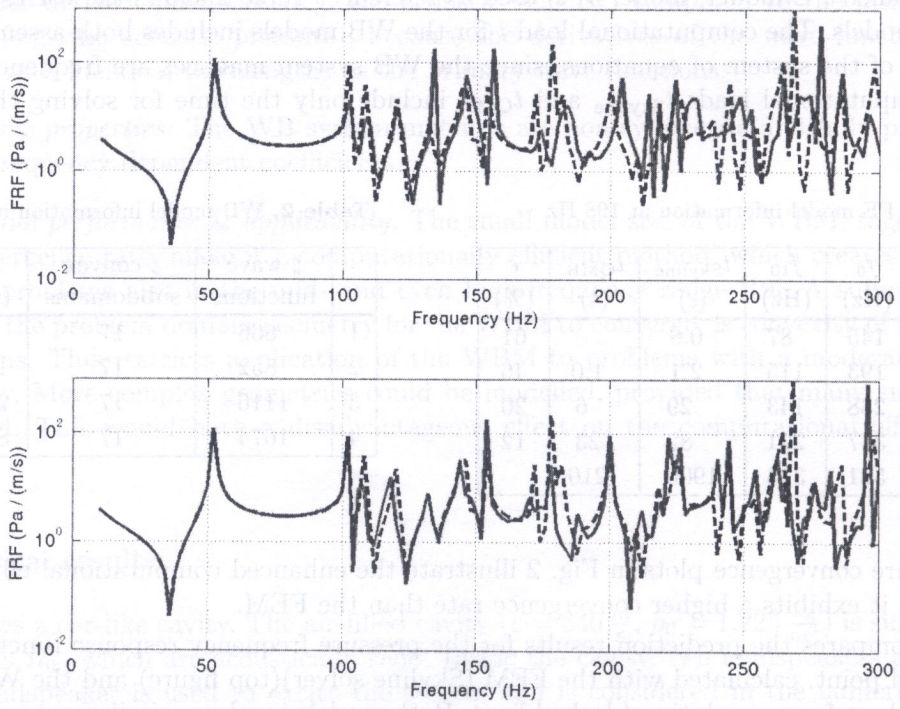

Fig. 3. Pressure FRF (amplitude): comparison of FE model 3 — Skyline solver (solid line, top figure) and WB model 3 (solid line, bottom figure) with a reference solution — FE model 5 (dashed line)

3. The hybrid FE-WB method

A restriction for efficient application of the WBM for general acoustic problems, is the required moderate complexity of the geometrical description of the considered acoustic problem domain. This section discusses the development of a hybrid FE-WB method, which overcomes this shortcoming. After a short description of the FEM basic concepts, the basic principles of the hybrid FE-WB method are discussed. In conclusion, a validation example illustrates the potential of the novel hybrid method.

3.1. The finite element method

3.1.1. Basic FEM concepts

In order to apply the FEM for the acoustic problem described in Section 2.1, the considered acoustic cavity V is subdivided into a number of non-overlapping finite elements V^e, $\left(V = \bigcup_{e=1}^{n_e} V^e \text{ with } V^i \bigcap V^j = \emptyset, \forall i \neq j\right)$, as is shown in Fig. 4. Corresponding to each element, a number of n_a^e nodes is defined at some particular locations in the element. The total number of nodes in the discretization is n_a. The boundary $\Omega^e = \partial V^e$ of each element V^e is composed of four non-overlapping parts $\left(\Omega^e = \Omega_p^e \bigcup \Omega_v^e \bigcup \Omega_Z^e \bigcup \Omega_i^e\right)$, namely those parts, which are intersections of the element boundary Ω^e with the problem boundary $\left(\Omega_p^e = \Omega^e \bigcap \Omega_p,\ \Omega_v^e = \Omega^e \bigcap \Omega_v,\ \Omega_Z^e = \Omega^e \bigcap \Omega_Z\right)$, and the common interface Ω_i^e between two adjacent elements.

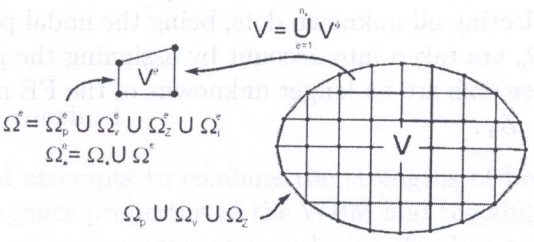

Fig. 4. A finite element discretization

Within each element V^e, the exact solution of the Helmholtz equation (1) is approximated by a linear combination of n_a^e simple (polynomial) element shape functions

$$p(\mathbf{r}) \simeq \hat{p}(\mathbf{r}) = \sum_{a=1}^{n_a^e} p_a^e N_a^e(\mathbf{r}), \qquad \mathbf{r} \in V_e. \tag{13}$$

Based on the element shape functions N_a^e, which are locally defined in one element V_e, some global shape functions N_a may be constructed, which are defined in the entire acoustic cavity V. In each element V_e to which node a belongs, the global shape function N_a is identical to the corresponding element shape function N_a^e, while it is zero in all other elements. In this way, a global pressure expansion may be defined as

$$p(\mathbf{r}) \simeq \hat{p}(\mathbf{r}) = \sum_{a=1}^{n_a} p_a N_a(\mathbf{r}) = \mathbf{N}(\mathbf{r})\,\mathbf{p_{fe}}, \qquad \mathbf{r} \in V. \tag{14}$$

The contribution factors p_a, stored in the element vector $\mathbf{p_{fe}}$, are the unknown element dofs. In general, the unknown dofs are nodal pressure values. The associated shape functions N_a are stored in the row vector $\mathbf{N}$.

Assume that the global pressure expansion (14) satisfies a priori both the pressure boundary conditions along Ω_p and the pressure continuity between two adjacent elements along their common

interface Ω_i^e (conforming elements). The pressure approximation violates the governing Helmholtz equation (1) within the acoustic cavity V, the normal velocity boundary condition along Ω_v, the impedance boundary condition along Ω_Z and the inter-element velocity continuity between two adjacent elements on Ω_i^e. The involved residuals on these relations are forced to zero in an integral sense by application of a weighted residual formulation. Contributions of the enforcement of the inter-element velocity continuity cancel out each other in this formulation, yielding the following weighted residual expression,

$$\int_V W_a \left(\nabla^2 \hat{p} + k^2 \hat{p}(\mathbf{r}) + j\rho_0 \omega\, \delta(\mathbf{r}, \mathbf{r_q})\, q\right) \mathrm{d}V + \int_{\Omega_v} j\rho_0 \omega\, W_a\, R_v(\hat{p})\, \mathrm{d}\Omega + \int_{\Omega_Z} j\rho_0 \omega\, W_a\, R_Z(\hat{p})\, \mathrm{d}\Omega = 0, \tag{15}$$

where W_a represents a weighting function. A Galerkin approach is adopted in that the weighting function W_a is expanded in a linear combination of the same shape functions N_a.

Substitution of expansion (14) in the weighted residual formulation (15) and application of integration by parts, yields an FE model

$$\mathbf{Z_a}\,\mathbf{p_{fe}} = \mathbf{f_a} \quad \text{with} \quad \mathbf{Z_a} = -\omega^2 \mathbf{M_a} + j\omega \mathbf{C_a} + \mathbf{K_a}, \quad \mathbf{f_a} = j\omega(\mathbf{q} - \mathbf{v_n}), \tag{16}$$

with $\mathbf{M_a}$, $\mathbf{C_a}$ and $\mathbf{K_a}$ the acoustic mass, damping and stiffness matrices. $\mathbf{q}$ and $\mathbf{v_n}$ represent loading vectors resulting from the acoustic point source q and the prescribed normal velocity $\bar{v}_n$. The vector $\mathbf{p_{fe}}$ is the solution vector, collecting all unknown dofs, being the nodal pressure values. The pressure boundary conditions along Ω_p are taken into account by assigning the prescribed values directly to the nodal dofs, such that these dofs are no longer unknowns of the FE model and can be condensed out of the FE system matrix $\mathbf{Z_a}$.

3.1.2. Model properties

Degrees of freedom: The dofs in an FE model are the nodal values $\mathbf{p_{fe}}$, usually representing nodal pressures.

Problem discretization & approximation functions: The FEM requires a discretization of the problem domain into small elements. Within these elements, approximating shape functions are used to describe the dynamic response variables. In order to yield prediction results with reasonable accuracy, element sizes have to decrease with increasing frequency, because wavelengths shorten.

Accuracy of secondary variables: Due to the fact that the primary response variables in the FEM are most commonly approximated with simple polynomial shape functions, the higher-order derived quantities are less accurate than the primary ones.

System matrix properties: The system matrices in the FEM are large and sparsely populated with real coefficients (unless complex model properties are introduced). They have a banded structure, are symmetric and can be decomposed into frequency independent submatrices (16). All of these properties allow computationally efficient storage and solution of the FE system of equations.

Computational performance & applicability: Because of the fine discretization of the FEM, the method has almost no restrictions regarding the geometrical complexity of the considered problem. However, due to the very large models at higher frequencies, computational resources restrict the use of the FEM to low-frequency applications.

3.2. FE and WB model properties comparison

Sections 2.3 and 3.1.2 describe the different model properties of the WBM and the FEM. Table 3 summarizes the main characteristics of the different methods, regarding their computational performance and general applicability.

The small model size of the WBM, together with the high convergence rate, make it a less computationally demanding method than the FEM, which creates opportunities for the WBM to tackle problems also in the mid- and even high-frequency range, while the FEM is restricted to low-frequency applications. However, because of the fine discretization of the FEM, it has almost no restrictions regarding the geometrical complexity of the considered problem, while the WBM is restricted to problems with a moderate geometrical complexity because of the recommended partitioning into large convex subdomains.

Table 3. Performance properties of different models (for acoustic analysis)

	FEM	WBM
matrix size	large	small
matrix building time	low	high
matrix system solution time	medium / high	low
convergence rate	medium	high
applicable frequency range	low	low, mid, (high)
problem geometry complexity	high	moderate

3.3. The hybrid FE-WB method

The hybrid FE-WB method attempts to combine the strengths of both the FEM and the WBM, namely the enhanced convergence properties of the WBM and the ability of the FEM to model any geometry, without restrictions on geometrical complexity. Applied to a general acoustic problem, large homogeneous acoustic domains are modelled with the WBM, while the geometrically more complex regions are tackled with the FEM.

In the following sections, a *direct* coupling approach is described. The term *direct* relates to the direct introduction of continuity conditions in both the FE and WB model along the common interface Ω_H. An alternative coupling approach is to apply an *indirect* coupling through the application of auxiliary frames [9]. Figure 5 introduces the fundamental notations for a *direct* hybrid coupling.

Three different *direct* couplings are identified, mutually distinguished by the applied continuity conditions:

- With a **pressure-velocity coupling**, the applied continuity conditions are formulated as $(\forall \mathbf{r} \in \Omega_H)$

$$\begin{aligned} v_{\mathrm{fe}}(\mathbf{r}) &= -v_{\mathrm{w}}(\mathbf{r}), \\ p_{\mathrm{w}}(\mathbf{r}) &= p_{\mathrm{fe}}(\mathbf{r}). \end{aligned} \tag{17}$$

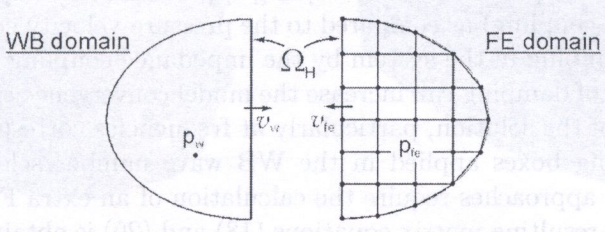

Fig. 5. A direct FE-WB coupling

The interface Ω_H between the WB and the FE domain imposes a velocity boundary condition on the FE domain and a pressure boundary condition on the WB domain. Extension of the weighted residual formulations (10) and (15) with the continuity conditions (17), yields the following matrix equation,

$$\begin{bmatrix} \mathbf{Z_a} & \mathbf{Q}_{\mathbf{fw}}^{(\mathbf{pv})} \\ \mathbf{Q}_{\mathbf{wf}}^{(\mathbf{pv})} & \mathbf{A} + \mathbf{C}_{\mathbf{b}}^{(\mathbf{pv})} \end{bmatrix} \begin{Bmatrix} \mathbf{p_{fe}} \\ \mathbf{p_a} \end{Bmatrix} = \begin{Bmatrix} \mathbf{f_a} + \mathbf{p}_{\mathbf{fw}}^{(\mathbf{pv})} \\ \mathbf{b} + \mathbf{c}_{\mathbf{b}}^{(\mathbf{pv})} \end{Bmatrix}, \tag{18}$$

with $\mathbf{Q}_{\mathbf{fw}}^{(\mathbf{pv})}$ and $\mathbf{Q}_{\mathbf{wf}}^{(\mathbf{pv})}$ coupling matrices, with $\mathbf{p}_{\mathbf{fw}}^{(\mathbf{pv})}$ a loading vector resulting from an acoustic point source q located in the WB domain, and with $\mathbf{C}_{\mathbf{b}}^{(\mathbf{pv})}$ and $\mathbf{c}_{\mathbf{b}}^{(\mathbf{pv})}$ WB back-coupling matrices.

- With an **impedance coupling (equivalent velocity coupling)**, the applied continuity conditions are formulated as follows ($\forall \mathbf{r} \in \Omega_H$),

$$\begin{aligned} v_{\mathrm{fe}}(\mathbf{r}) - p_{\mathrm{fe}}(\mathbf{r})/\bar{Z} &= -v_{\mathrm{w}}(\mathbf{r}) - p_{\mathrm{w}}(\mathbf{r})/\bar{Z}, \\ v_{\mathrm{w}}(\mathbf{r}) - p_{\mathrm{w}}(\mathbf{r})/\bar{Z} &= -v_{\mathrm{fe}}(\mathbf{r}) - p_{\mathrm{fe}}(\mathbf{r})/\bar{Z}, \end{aligned} \tag{19}$$

with $\bar{Z}$ a coupling impedance value which can be chosen freely. Equations (19) are a linear combination of Eqs. (17). Previous research addressed the application of a similar impedance coupling for the coupling of two WB domains [18]. It was shown that the particular selection of the characteristic acoustic impedance $\bar{Z} = \rho_0 c$ yields good results.

Ω_H imposes an impedance boundary condition on both the FE and WB domain. The weighted residual formulations of both the WB model and the FE model, (10) and (15) respectively, are extended and yield the following matrix equation,

$$\begin{bmatrix} \mathbf{Z_a} + j\omega \mathbf{C}_{\mathbf{f}}^{(\mathbf{imp})} & \mathbf{Q}_{\mathbf{fw}}^{(\mathbf{imp})} \\ \mathbf{Q}_{\mathbf{wf}}^{(\mathbf{imp})} & \mathbf{A} + \mathbf{C}_{\mathbf{b}}^{(\mathbf{imp})} \end{bmatrix} \begin{Bmatrix} \mathbf{p_{fe}} \\ \mathbf{p_a} \end{Bmatrix} = \begin{Bmatrix} \mathbf{f_a} + \mathbf{p}_{\mathbf{fw}}^{(\mathbf{imp})} \\ \mathbf{b} + \mathbf{c}_{\mathbf{b}}^{(\mathbf{imp})} \end{Bmatrix}, \tag{20}$$

with $\mathbf{C}_{\mathbf{f}}^{(\mathbf{imp})}$ an FE back-coupling matrix.

- With a **mixed impedance-pressure coupling**, the applied continuity conditions are formulated as ($\forall \mathbf{r} \in \Omega_H$)

$$\begin{aligned} v_{\mathrm{fe}}(\mathbf{r}) - p_{\mathrm{fe}}(\mathbf{r})/\bar{Z} &= -v_{\mathrm{w}}(\mathbf{r}) - p_{\mathrm{w}}(\mathbf{r})/\bar{Z} \\ p_{\mathrm{w}}(\mathbf{r}) &= p_{\mathrm{fe}}(\mathbf{r}) \end{aligned} \tag{21}$$

Equations (21) are also a linear combination of equations (17). Ω_H imposes an impedance boundary condition on the FE domain and a pressure boundary condition on the WB domain. The weighted residual formulations of the FE and WB model are extended and yield a matrix equation similar to (20).

The advantage of the two impedance based coupling approaches (the impedance coupling and the mixed impedance-pressure coupling) as compared to the pressure-velocity coupling, is the possibility to artificially introduce damping in the system by the impedance coupling factor $\bar{Z}$. [18] has shown that artificial introduction of damping can increase the model convergence speed and has a beneficial influence on the stability of the solution, particularly at frequencies corresponding to the resonance frequencies of the bounding boxes applied in the WB wave number selection (8). However, the impedance based coupling approaches require the calculation of an extra FE back-coupling matrix.

Efficient solution of the resulting matrix equations (18) and (20) is obtained through a three-step solution procedure:

1. First the FE dofs are eliminated from the system of equations by application of a sparse matrix solver. For Eq. (18), this yields

$$\left[-\mathbf{Q}_{\mathrm{wf}}^{(\mathrm{pv})}\,\mathbf{H}^{(\mathrm{pv})}+\mathbf{A}+\mathbf{C}_{\mathrm{b}}^{(\mathrm{pv})}\right]\{\mathbf{p}_{\mathrm{a}}\}=\left\{\mathbf{b}+\mathbf{c}_{\mathrm{b}}^{(\mathrm{pv})}-\mathbf{Q}_{\mathrm{wf}}^{(\mathrm{pv})}\,\mathbf{h}^{(\mathrm{pv})}\right\} \tag{22}$$

where the auxiliary matrix $\mathbf{H}^{(\mathrm{pv})}$ and the auxiliary vector $\mathbf{h}^{(\mathrm{pv})}$ are obtained by solving the following sparse linear systems,

$$\mathbf{Z}_{\mathrm{a}}\,\mathbf{H}^{(\mathrm{pv})}=\mathbf{Q}_{\mathrm{fw}}^{(\mathrm{pv})}\quad\text{and}\quad\mathbf{Z}_{\mathrm{a}}\,\mathbf{h}^{(\mathrm{pv})}=\mathbf{f}_{\mathrm{a}}+\mathbf{p}_{\mathrm{fw}}^{(\mathrm{pv})}\,. \tag{23}$$

2. In a second step, the remaining, dense, but much smaller, matrix equation is solved with a dense solver to obtain the wave function contribution factors.

3. After solution of the dense system, the FE dofs are retrieved by simple matrix multiplications

$$\mathbf{p}_{\mathrm{fe}}=-\mathbf{H}^{(\mathrm{pv})}\,\mathbf{p}_{\mathrm{a}}+\mathbf{h}^{(\mathrm{pv})}. \tag{24}$$

Such a condensation approach is common for hybrid Trefftz methods [6, 15], where the dofs related to the interior field description are eliminated and a smaller system, consisting of the applied Lagrangian multipliers, is retained for solution.

3.4. Numerical results

Consider the interior acoustic cavity of a car, shown in Fig. 6. The air-filled ($c = 340\,\frac{\mathrm{m}}{\mathrm{s}}$, $\rho_0 = 1.225\,\frac{\mathrm{kg}}{\mathrm{m}^3}$) cavity is surrounded by acoustically rigid panels. The system is excited by an acoustic point source q with a power of 1 W, located at the right firewall panel.

The performances of the FEM and the hybrid FE-WB method are compared for this validation case. Figure 6 shows the full car cavity as it is modelled with FE. The applied FE models consist of 4-noded linear tetrahedral elements and the solution code is *MSC/Nastran2004*. Figure 7 shows a hybrid model of the same car cavity. A large, geometrically simple, convex volume is now modelled with a single WB domain, while the remaining fraction (11%) of the cavity, located near the firewall panels, is modelled with FE. The hybrid FE-WB routines are implemented in a C++ code. To compare the computational performance of both methods, all calculations are performed on the same 3 GHz Intel Pentium 4 system, running a Linux operating system.

To illustrate that the interface continuity conditions are met, Fig. 8 shows the pressure amplitude contour plot at 150 Hz, calculated with the *direct* pressure-velocity coupling. This figure illustrates that the pressure field is continuous over the coupling interface Ω_H. Furthermore, the rigid outer

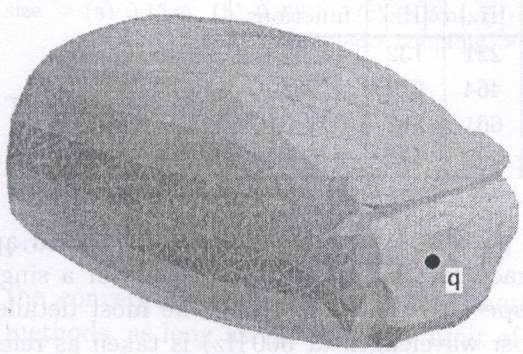

Fig. 6. An interior car cavity

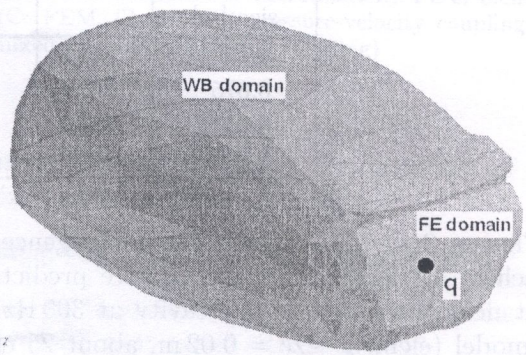

Fig. 7. A hybrid FE-WB model

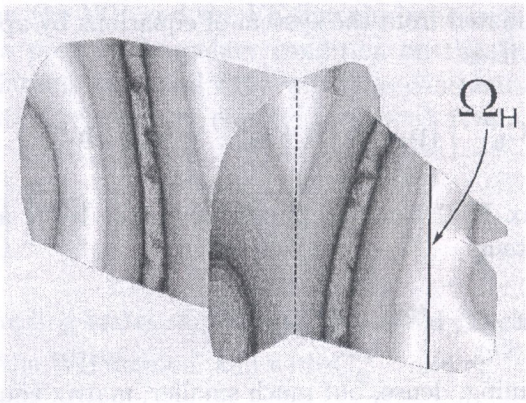

Fig. 8. Contour plot of the pressure amplitude at 150 Hz, calculated with the *direct* pressure-velocity coupling

panels are correctly taken into account, since the pressure contour lines are perpendicular to the rigid panels.

In order to illustrate the enhanced convergence properties of the hybrid FE-WB method compared to the FEM, and in order to compare the performance of the three different *direct* coupling approaches, a pressure convergence analysis (12) is performed for a point near the centre of the cavity. Tables 4 and 5 summarize the model information of the numerical models applied in the convergence analysis. f_6 and f_{10} indicate the upper limits of the frequency ranges for which the FE mesh includes at least 6 and 10 linear elements per wavelength, respectively.

Table 4. FE model information at 300 Hz

element size [m]	♯ nodes	♯ elements	f_6 [Hz]	f_{10} [Hz]
0.15	4850	24362	223	134
0.10	11147	58280	283	170
0.06	36929	202254	495	297
0.05	54789	303276	462	277
0.04	95558	534066	611	367
0.035	135098	762070	646	387
0.0275	252216	1440912	949	570
0.02	509817	2927228	1021	613

Table 5. Hybrid FE-WB model information at 300 Hz

FE element size [m]	♯ nodes	♯ elements	f_6 [Hz]	f_{10} [Hz]	♯ wave functions
0.15	591	2268	221	132	112
0.075	3399	16246	464	279	288
0.05	8056	40920	661	397	288
0.0275	31940	171740	962	577	586

Figures 9(a)–(d) compare the convergence rates of the FEM and the three *direct* hybrid approaches. All figures plot the relative prediction accuracy for the pressure amplitude of a single point near the centre of the cavity at 300 Hz, with respect to the CPU time. The most detailed FE model (element size = 0.02 m, about 25 elements per wavelength at 300 Hz) is taken as reference model for the convergence analysis. Each figure plots the FE convergence curve (dashed line), and the hybrid FE-WB convergence curves obtained with hybrid models of which the FE part has

a fixed element size (cfr. the first column of Table 5) and of which the number of wave functions is increased. The hybrid FE-WB curves have an elbow shape. The number of wave functions listed in the last column of Table 5, denotes the number of wave functions at the hinge of the elbow. Note that all the indicated CPU times for the frequency independent FE models include only the time for solution of the system, while the CPU times for the frequency dependent hybrid models include both the times for assembly and solution of the system of equations.

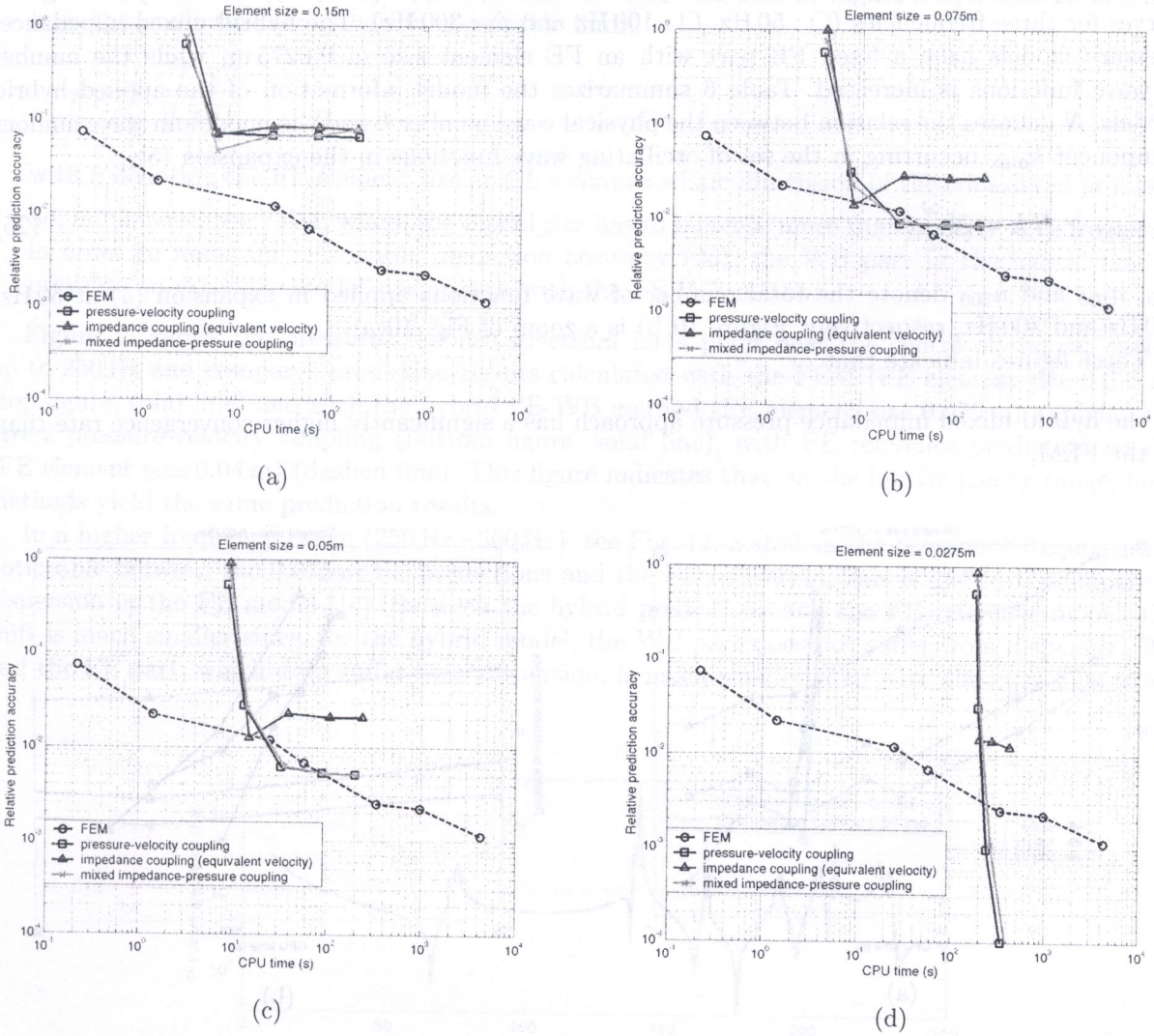

Fig. 9. Pressure convergence curves at 300 Hz for hybrid models with different FE discretizations: FE element size = (a) 0.15 m, (b) 0.075 m, (c) 0.05 m, (d) 0.0275 m (○: FEM, □: FE-WB pressure-velocity coupling, △: FE-WB impedance coupling, ×: FE-WB mixed impedance-pressure coupling)

These figures show that

- for a fixed FE discretization, with increasing number of wave functions, the accuracy of the hybrid models stagnates because of the accuracy limit of the involved FE part,
- prediction results become more accurate when refining the FE part of the hybrid models,
- the convergence rate of the hybrid methods is higher than the convergence rate of the FE methods, as long as the accuracy limit of the involved FE part is not reached,
- the pressure-velocity coupling and the mixed impedance-pressure coupling yield similar convergence curves,

- the impedance coupling has a similar convergence rate as the two other *direct* couplings, but stagnates before the other couplings do,
- the choice of the coupling impedance value $\bar{Z}$ to be the characteristic acoustic impedance $\rho_0 c$, yields good results for the mixed impedance-pressure coupling.

To illustrate the potential of the hybrid FE-WB methods for tackling mid-frequency applications, Fig. 10(a) plots the FE (dashed lines) and hybrid mixed impedance-pressure (solid lines) convergence curves for three frequencies (○ : 50 Hz, □ : 100 Hz and △ : 300 Hz). The hybrid mixed impedance-pressure models have a fixed FE part with an FE element size of 0.0275 m, while the number of wave functions is increased. Table 6 summarizes the model information of the applied hybrid models. N denotes the relation between the physical wave number k and the maximum wave number component $k_{\max}$ occurring in the set of oscillating wave functions in the expansion (5),

$$k_{\max} \geq N\,k = N\,\frac{\omega}{c}\,, \tag{25}$$

n_{50}, n_{100} and n_{300} denote the total number of wave functions applied in expansion (5) at 50 Hz, 100 Hz and 300 Hz, respectively. Figure 10(b) is a zoom of Fig. 10(a).

These figures indicate that

- the hybrid mixed impedance-pressure approach has a significantly higher convergence rate than the FEM,

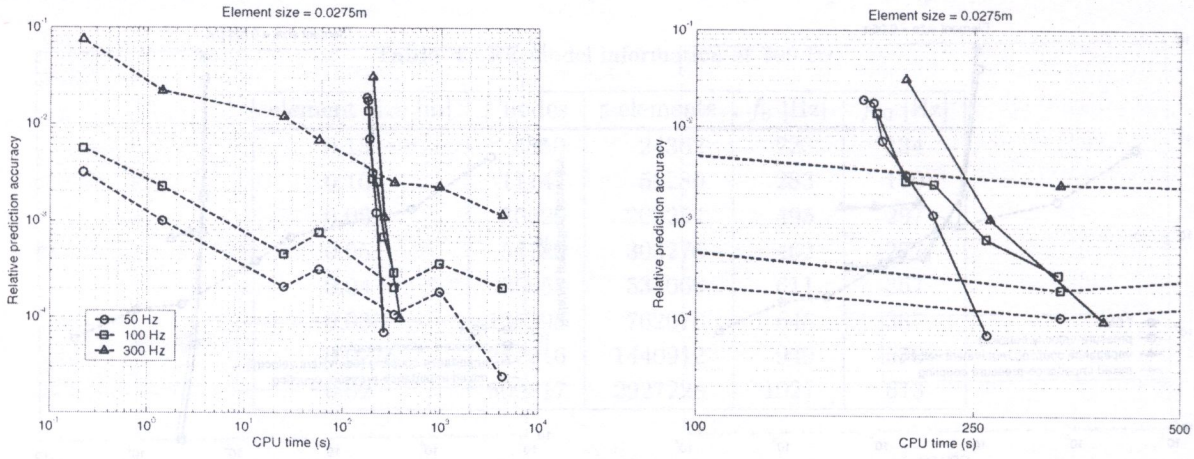

(a) (b)

Fig. 10. Pressure convergence curves the FEM (dashed lines) and the hybrid mixed impedance-pressure approach with a fixed FE discretization (FE element size = $0.0275m$)(solid lines) at ○: 50 Hz, □: 100 Hz and △: 300 Hz

Table 6. Hybrid FE-WB model information (FE element size = 0.0275 m)

N	n_{50}	n_{100}	n_{300}
1		32	112
2	32	66	288
3	54	112	586
4	66	166	
6	112	288	
8	166		
12	288		

- with increasing frequency, the accuracy level of the FE predictions deteriorates, since the dashed lines shift upwards with increasing frequency,
- with increasing frequency, the parameter N in Eq. (25) can decrease, while still yielding accurate predictions. This behaviour illustrates the potential of the hybrid FE-WB method for tackling problems in the mid- and high-frequency range. For the FEM, [14] and [1] have shown that applying the rule of thumb of using a fixed number of elements per wavelength is only valid at low frequencies and proposed application of the following rule at higher frequencies in order to keep the prediction errors within acceptable limits

$$f < \frac{c}{2\pi}\sqrt[3]{\frac{1}{L\,h^2}} \tag{26}$$

with h denoting the FE element size and L a characteristic dimension of the considered problem. So, unlike with the FEM, where the model size has to increase more than linearly with frequency in order to maintain reasonable prediction accuracy (26), the WB part in the hybrid models prevents an excessive model size growth with the FE-WB method.

Figure 11 shows the pressure response spectrum for a point near the centre of the car cavity, up to 250 Hz and compares prediction results calculated with the FEM (FE element size 0.075 m) (top figure, solid line) and with the hybrid FE-WB method (FE element size 0.075 m) applying the *direct* pressure-velocity coupling (bottom figure, solid line), with FE reference prediction results (FE element size 0.04 m) (dashed line). This figure indicates that, in the low frequency range, both methods yield the same prediction results.

In a higher frequency range (250 Hz – 500 Hz), see Fig. 12, a shift in the resonance frequencies is noticeable between the 0.075 m FE predictions and the FE reference. This is due to the numerical dispersion in the FE model [14]. Between the hybrid predictions and the FE reference model, the shift is much smaller since, for the hybrid model, the WB part does not suffer from dispersion [22] and the FE part, which does suffer from dispersion, is much smaller than with the pure FE model.

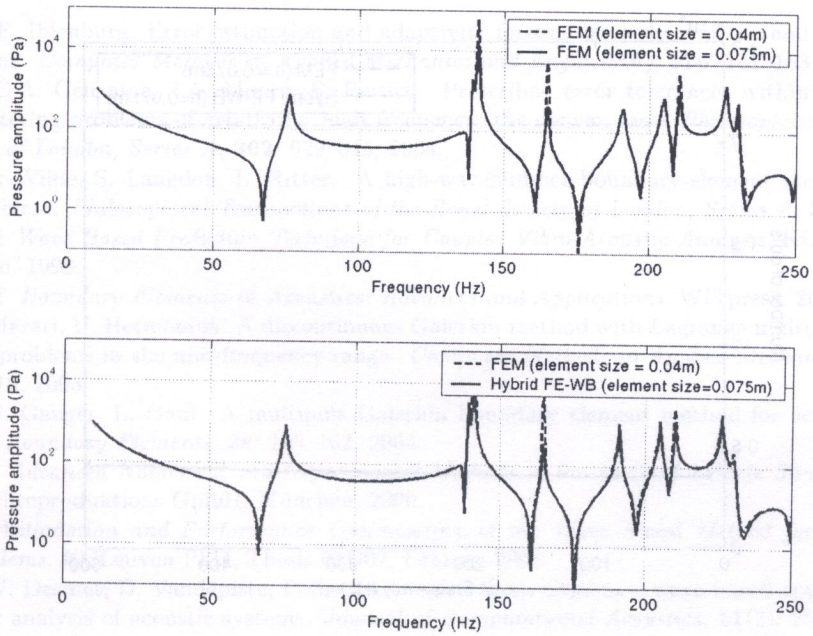

Fig. 11. Pressure amplitude response spectrum (Pa), dashed line: FE reference, solid line top figure: FEM predictions, solid line bottom figure: hybrid predictions

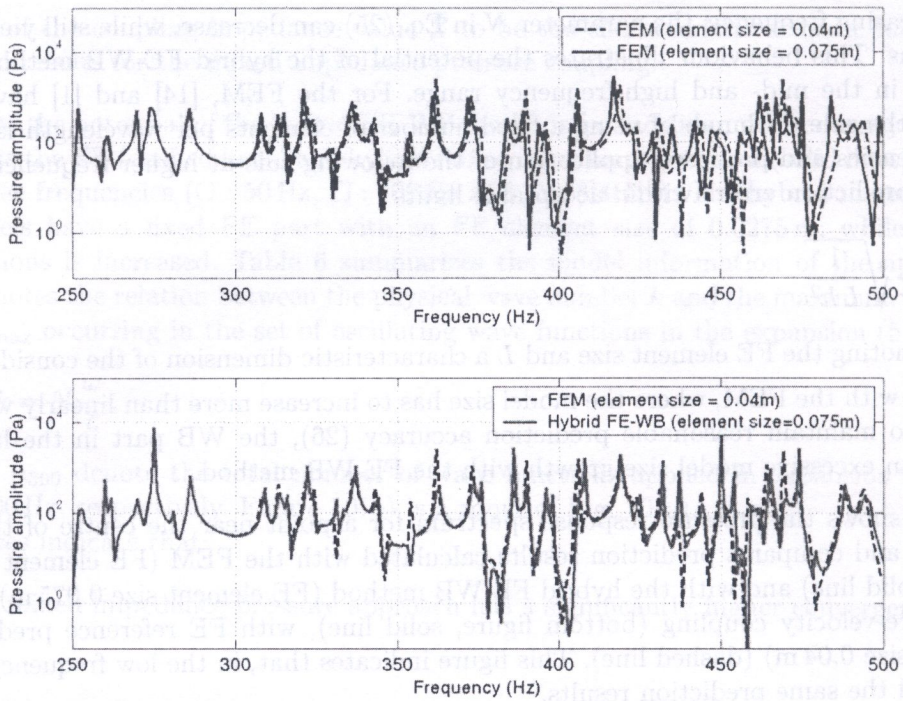

Fig. 12. Pressure amplitude response spectrum (Pa), dashed line: FE reference, solid line top figure: FEM predictions, solid line bottom figure: hybrid predictions

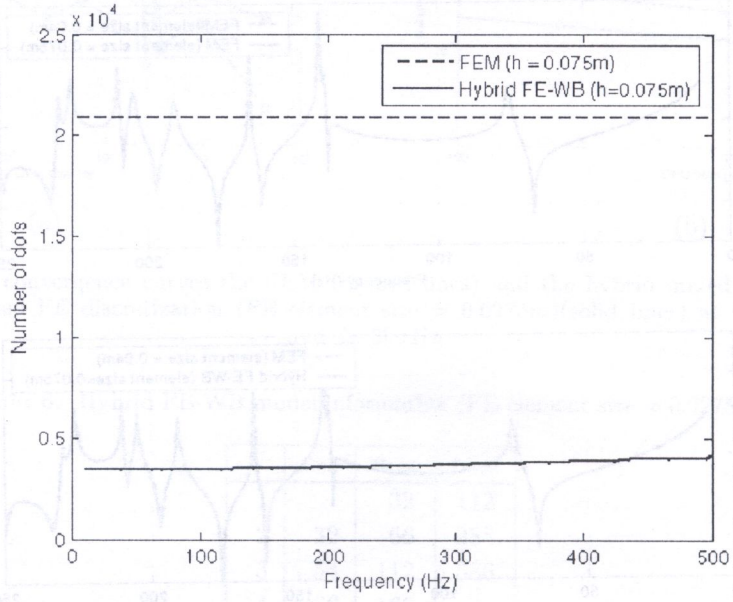

Fig. 13. Number of dofs, dashed line: FE model $h = 0.075\,\mathrm{m}$, solid line: hybrid FE-WB model $h = 0.075\,\mathrm{m}$

Figure 13 illustrates that, besides the reduced dispersion, the hybrid FE-WB model is also much smaller than the corresponding FE model. The dotted line represents the model size of the FE model with $h = 0.075$ applied for the prediction of the response functions in Figs. 11 and 12. The solid line represents the total number of dofs of the hybrid FE-WB model with $h = 0.075$, which consists of a constant number of FE dofs, i.e. 3399, and an increasing number of wave functions, i.e. a minimum of 24 functions at 10 Hz and a maximum of 712 functions at 500 Hz.

4. Conclusions

This paper illustrates the applicability of both the WBM and the hybrid FE-WB method for interior acoustic analysis.

In the first part of the paper, the enhanced convergence characteristics of the WBM are illustrated by means of the acoustic analysis of a 3D cavity of moderate geometrical complexity.

A second part of the paper discusses the development of a hybrid FE-WB method. By combining the high performance characteristics of the WBM and the ability of the FEM to model any problem, regardless of its geometrical complexity, the hybrid method becomes an efficient, generally applicable method. Mutually distinguished by the applied continuity conditions, three different *direct* hybrid FE-WB methods are discussed and their performance is illustrated by means of the acoustic analysis of an interior car cavity.

Acknowledgments

The research work is carried out in the framework of the research project *TRICARMO* and the scholarships of Bert Pluymers and Caroline Vanmaele, which are financed by the Institute for the Promotion of Innovation by Science and Technology in Flanders (IWT). The support of the Flemish government is gratefully acknowledged.

References

[1] P. Bouillard, F. Ihlenburg. Error estimation and adaptivity for the finite element method in acoustics: 2D and 3D applications. *Computer Methods in Applied Mechanics and Engineering*, **176**: 147–163, 1999.

[2] O.P. Bruno, C.A. Geuzaine, J.A. Monro, F. Reitich. Prescribed error tolerances within fixed computational times for scattering problems of arbitrarily high frequency: the convex case. *Philosophical Transactions of the Royal Society of London, Series A*, **362**: 629–645, 2004.

[3] N.S. Chandler-Wilde, S. Langdon, L. Ritter. A high-wavenumber boundary-element method for an acoustic scattering problem. *Philosophical Transactions of the Royal Society of London, Series A*, **362**: 647–671, 2004.

[4] W. Desmet. *A Wave Based Prediction Technique for Coupled Vibro-Acoustic Analysis.* KULeuven PhD. Thesis 98D12, Leuven, 1998.

[5] O. von Estorff. *Boundary Elements in Acoustics: Advances and Applications.* WITpress, 2000.

[6] C. Farhat, I. Harari, U. Hetmaniuk. A discontinuous Galerkin method with Lagrange multipliers for the solution of Helmholtz problems in the mid-frequency range. *Computer Methods in Applied Mechanics and Engineering*, **192**: 1389–1419, 2003.

[7] M. Fischer, U. Gauger, L. Gaul. A multipole Galerkin boundary element method for acoustics. *Engineering Analysis with Boundary Elements*, **28**: 155–162, 2004.

[8] R. Freymann. *Advanced Numerical and Experimental Methods in the Field of Vehicle Structural-Acoustics.* Hieronymus Buchreproduktions GmbH, München, 2000.

[9] B. van Hal. *Automation and Performance Optimization of the Wave Based Method for Interior Structural-Acoustic Problems.* KULeuven PhD. Thesis 04D07, Leuven, 2004.

[10] B. van Hal, W. Desmet, D. Vandepitte, P. Sas. A coupled finite element – wave based approach for the steady state dynamic analysis of acoustic systems. *Journal of Computational Acoustics*, **11**(2): 255–283, 2003.

[11] B. van Hal, W. Desmet, D. Vandepitte, P. Sas. Hybrid finite element – wave based method for acoustic problems. *Computer Assisted Mechanics and Engineering Sciences (CAMES)*, **11**: 375–390, 2003.

[12] D. Huybrechs, S. Vandewalle. *A Sparse Discretisation for Integral Equation Formulations of High Frequency Scattering Problems.* K.U.Leven, Technisch rapport TW-447, 2006.

[13] F. Ihlenburg, I. Babuska. Finite element solution to the Helmholtz equation with high wavenumber. Part I: The h-version of the FEM. *Computational Methods in Applied Mechanical Engineering*, **30**: 9–37, 1995.

[14] F. Ihlenburg. *Finite Element Analysis of Acoustic Scattering. Applied Mathematical Sciences*, **132**: Springer, 1998.

[15] J. Jirousek, A. Wróblewski. T-elements: state-of-the-art and future trends. *Archives of Computational Methods in Engineering*, **3**: 323–434, 1996.

[16] R.H. Lyon, R.G. DeJong. *Theory and Application of Statistical Energy Analysis. Second Edition.* Butterworth–Heinemann, Boston, 1995.

[17] E. Perrey-Debain, J. Trevelyan, P. Bettess. Wave boundary elements: a theoretical overview presenting applications in scattering of short waves. *Engineering Analysis with Boundary Elements*, **28**: 131–141, 2004.

[18] B. Pluymers, W. Desmet, D. Vandepitte, P. Sas. A Trefftz-based prediction technique for multi-domain steady-state acoustic problems. *Proceedings of the Tenth International Congress on Sound and Vibration*, Stockholm, Sweden, 2003.

[19] B. Pluymers, W. Desmet, D. Vandepitte, P. Sas. Feasibility study of the wave based method for high-frequency steady-state acoustic analysis. *Proceedings of the International Conference on Noise and Vibration Engineering ISMA2004*, Leuven, Belgium, 1555–1574, 2004.

[20] B. Pluymers, W. Desmet, D. Vandepitte, P. Sas. Application of an efficient wave based prediction technique for the analysis of vibro-acoustic radiation problems. *Journal of Computational and Applied Mathematics (JCAM)*, **168**: 353–364, 2004.

[21] B. Pluymers, W. Desmet, D. Vandepitte, P. Sas. On the use of a wave based prediction technique for steady-state structural-acoustic radiation analysis. *Journal of Computer Modeling in Engineering & Sciences (CMES)*, **7**(2): 173–184, 2005.

[22] B. Pluymers, A. Hepberger, W. Desmet, H.H. Priebsch, D. Vandepitte, P. Sas. Experimental validation of the wave based prediction technique for the analysis of the coupled vibro-acoustic behaviour of a 3D cavity. *Proceedings of the Second MIT Conference on Solid and Fluid Mechanics (MIT2)*, Boston, Massachusetts, USA, 1483–1487, 2003.

[23] S. Schneider. Application of fast methods for acoustic scattering and radiation problems. *Journal of Computational Acoustics*, **11**: 387–401, 2003.

[24] E. Trefftz. Ein Gegenstück zum Ritzschen Verfahren. *Proceedings of the 2nd International Congress on Applied Mechanics*, Zürich, Switzerland, 131–137, 1926.

[25] O.C. Zienkiewicz, R.L. Taylor. *The Finite Element Method – Vol. 1: Basic formulation and linear problems (fifth edition).* McGraw–Hill, London, 2000.